ISSN 0021-3640, JETP Letters, 2014, Vol. 99, No. 3, pp. 149–152. © Pleiades Publishing, Ltd., 2014.
Original Russian Text © A.M. Gazizulina, E.M. Alakshin, E.I. Baibekov, R.R. Gazizulin, M.Yu. Zakharov, A.V. Klochkov, S.L. Korableva, M.S. Tagirov, 2014, published in Pis'ma v Zhurnal Eksperimental'noi i Teoreticheskoi Fiziki, 2014, Vol. 99, No. 3, pp. 169–172.

Electron Paramagnetic Resonance of Gd^{3+} Ions in Powders of LaF_3:Gd^{3+} Nanocrystals

A. M. Gazizulina, E. M. Alakshin, E. I. Baibekov, R. R. Gazizulin, M. Yu. Zakharov, A. V. Klochkov, S. L. Korableva, and M. S. Tagirov

Institute of Physics, Kazan (Volga Region) Federal University, Kazan, 420008 Russia

e-mail: murat.tagirov@kpfu.ru

Received December 30, 2013

The observation of electron paramagnetic resonance of Gd^{3+} ions in nanosized powders of rare-earth fluorides LaF_3:Gd^{3+} has been reported. The measurements have been performed on a single crystal and micro- and nanosized powders at room temperature. Electron paramagnetic resonance spectra and spin-Hamiltonian parameters of Gd^{3+} ions have been obtained. A qualitative difference of spectra in nano- and micropowders due to the increase in the spread of the crystal field parameters with the decrease in the particle size has been found. The relationship between the single-crystal domain size and the hydrothermal treatment time has been established.

DOI: 10.1134/S0021364014030084

In this work, we studied nanosized powders of rare-earth trifluoride LaF_3 activated by Gd^{3+} ions. It is known that Gd^{3+} ions have no orbital angular momentum in the states of the lower $^3S_{7/2}$ multiplet. Consequently, the spin–lattice relaxation time of these states is rather long for the electron paramagnetic resonance signal to be observed at room temperature. This is the origin of gadolinium compounds being promising contrast agents in magnetic resonance tomography [1–3]. At present, contrast agents on the basis of rare-earth ions with the optimal structural and physicochemical properties making it possible to achieve the maximal contrast of the magnetic resonance tomography image are actively being sought [2, 4].

One of the simplest methods of the synthesis of nanosized powders is the method of deposition from colloid solutions. The structure and sizes of the synthesized particles can be controlled by the variation of the temperature and time of hydrothermal treatment [5]. To this end, a colloid solution with nanoparticles is placed in a microwave oven (the radiation power of ~650 W, the treatment time τ varying from 20 min to several hours). Recently, a new technique of varying the nanoparticle sizes of isostructural compounds (praseodymium trifluoride PrF_3) by varying the hydrothermal treatment time was tested [6, 7]. The increase in the nanoparticle sizes and ordering of their crystal structure were observed with increasing τ. Note two more interesting effects directly associated with the specificity of the structure of PrF_3 nanoparticles. Water clusters were detected in PrF_3 nanoparticles using electron microscopy and nuclear magnetic resonance [8]. The correlation of the nuclear magnetic relaxation parameters of ^{3}He and nanoparticle sizes was revealed for PrF_3 nanopowders in contact with liquid helium-3. [9].

In this work, we present the spectral study of a series of LaF_3 samples with the content of 0.5% of impurity Gd^{3+} ions. A single crystal was grown by the Bridgman–Stockbarger method. The micropowder was prepared by cutting a single crystal in a sapphire mortar and the subsequent sieving through a sieve. The particle size was 10–45 μm. Nanopowders were synthesized by the method of deposition from colloid solutions and subjected to the hydrothermal treatment. Lanthanum trifluoride was doped with gadolinium as follows. Gadolinium oxide (0.5%) was added to lanthanum oxide dissolved in nitric acid (99%). The prepared solution was carefully stirred. Then, the synthesis was performed as above [5]. Four samples nos. 1–4 were synthesized with treatment times $\tau = 0$, 20, 40, and 420 min, respectively. The X-ray analysis identified the samples as LaF_3. Electron paramagnetic resonance spectra were measured on an ESP-300 spectrometer (Bruker) in the *X* band (9.6 GHz) at a temperature of 300 K. Figures 1–5 show the measurement results.

To interpret the measured spectra, we write the spin Hamiltonian of the ground state $^8S_{7/2}$ of the Gd^{3+} ion in the magnetic field $\mathbf{B} = \mathbf{B}_0 + \mathbf{B}_1\cos(\omega t)$:

$$H = g\mu_B\mathbf{B}\cdot\mathbf{S} + \sum_{\substack{p = 2,4,6,\\ k = -p,\ldots,p}} B_p^k O_p^k, \qquad (1)$$

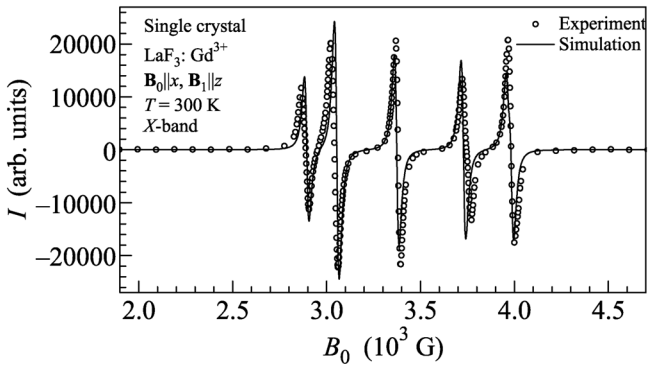

Fig. 1. Electron paramagnetic resonance spectrum of Gd^{3+} ions in the LaF_3:Gd^{3+} single crystal ($\mathbf{B}_0 \| x$ and $\mathbf{B}_1 \| z$).

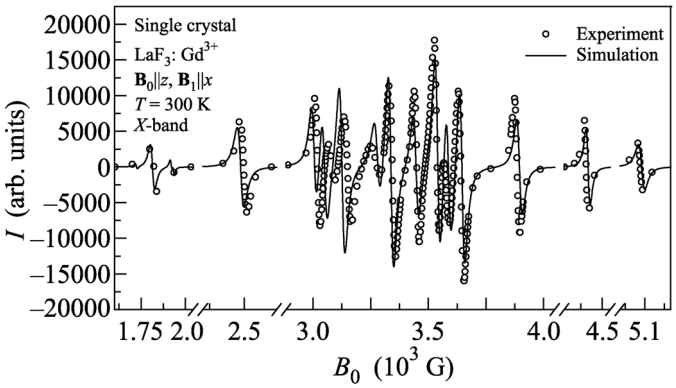

Fig. 2. Electron paramagnetic resonance spectrum of Gd^{3+} ions in the LaF_3:Gd^{3+} single crystal ($\mathbf{B}_0 \| z$ and $\mathbf{B}_1 \| x$).

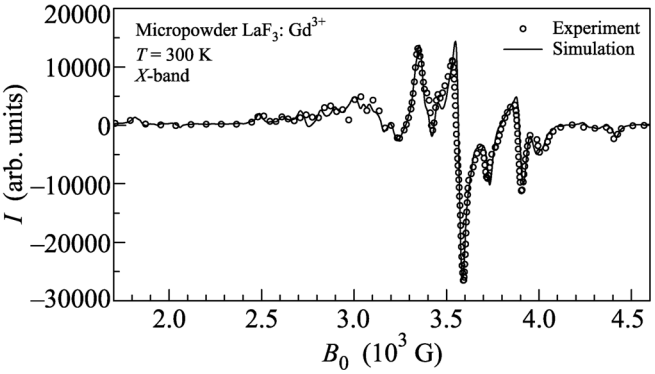

Fig. 3. Electron paramagnetic resonance spectrum of Gd^{3+} ions in the LaF_3:Gd^{3+} micropowder.

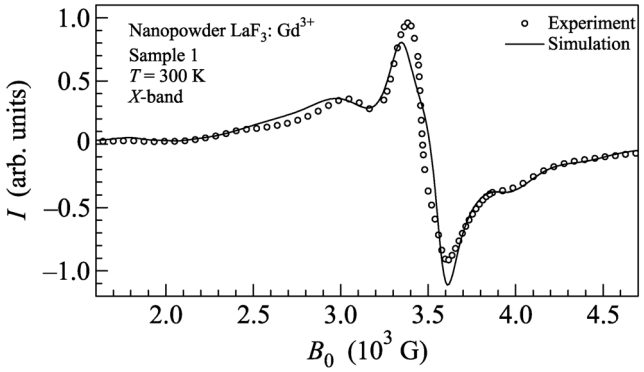

Fig. 4. Electron paramagnetic resonance spectrum of Gd^{3+} ions in the LaF_3:Gd^{3+} nanopowder (sample no. 1).

where the isotropic g-factor and crystal field parameters B_p^k serve as fitting parameters, O_p^k are Stevens operators [10], and μ_B is the Bohr magneton. The coordinate system from [11] was used in calculations: the x axis was oriented along the c axis of the regular LaF_3 crystal, and the z axis was chosen along the a axis. Several sets of crystal field parameters close to each other and describing well the electron paramagnetic resonance spectra for the orientations $\mathbf{B}_0 \| x$ and $\mathbf{B}_0 \| z$ are known [11, 12]. It is assumed that the local symmetry of the environment of the impurity Gd^{3+} ion substituting for the La^{3+} ion is orthorhombic and there are three types of nonequivalent substitution centers [12]. The latter determines the presence of the additional lines in the spectrum in Fig. 2.

However, as follows from our calculations using the combination of parameters from [11, 12], the agreement with the micropowder spectrum (Fig. 3) containing contributions from all possible orientations of the $\mathbf{B}_0$ vector with respect to the crystallographic axes is not satisfactory. In order to improve this agreement, we fitted the parameters B_p^k and g, which are given in the table. In our calculations, we proceeded from the parameters obtained in [13], where the spectra for the $\mathbf{B}_0$ orientations in the (xy) and (yz) planes were also considered. As in that work, it occurred that the inclusion of the parameters B_p^k in the calculation does not improve the agreement with the measured spectra. Therefore, they were taken to be zero. It is remarkable that the parameter $B_4^{-2} = 0.33 \times 10^{-4}$ cm^{-1} characterizing the local symmetry below orthorhombic is nonzero: attempts at describing the fine details of the micropowder spectrum disregarding this contribution did not succeed. At the same time, the obtained parameter set describes well the spectra of the regular crystal at the orientations $\mathbf{B}_0 \| x$ (Fig. 1) and $\mathbf{B}_0 \| z$ (Fig. 2).

The line shape of the electron paramagnetic resonance spectrum is close to Lorentzian. The question of why it is Lorentzian is a subject of a separate study. For the regular crystal and micropowder, the half-width of all lines was the same and was 21 G (here and below, it

is the half-width of the integral absorption curve). Apparently, the main contribution to the line width in these samples is due to the superhyperfine interaction between the gadolinium ions and the surrounding fluorine ions from the crystal lattice of LaF_3. Since the sizes of particles in nanopowders are tens of nanometers, the crystal field acting on the impurity center depends on the particle shape and size and the closeness of its boundaries. The spread of the parameters B_p^k near their equilibrium values presented in the table occurs and, as a consequence, the spread of the splittings of the energy levels of the ground state of Gd^{3+} ions appears. This leads to the increase in the half-width of the electron paramagnetic resonance lines, which is different for the central line ($-1/2 \leftrightarrow 1/2$ transition) and all other lines of the spectrum. In fact, it follows from the theoretical considerations in the first order of perturbation theory that the crystal field causes the same shift of the energy of states with the spin projections M and $-M$ on the direction of the field $\mathbf{B}_0$:

$$\delta E_M^{(1)} = \left\langle M \left| \sum_{pk} B_p^k O_p^k \right| M \right\rangle = \left\langle -M \left| \sum_{pk} B_p^k O_p^k \right| -M \right\rangle. \quad (2)$$

Consequently, the change of the transition energy $-1/2 \leftrightarrow 1/2$ due to the crystal field effect in comparison with its value $g\mu_B B$ for the free ion is only in the subsequent order of magnitude and its absolute value is much less. The spread of these energies due to the random shifts of the parameters B_k^p in nanocrystals will be less as well. It is reasonable to introduce two quantities for them, Δ_1 and Δ_2, characterizing the half-widths of the central line and transitions $\pm 1/2 \leftrightarrow \pm 3/2$ located close to the central part of the spectrum, respectively; these quantities satisfy the inequality $\Delta_1 < \Delta_2$. These two quantities were the only fitting parameters in the calculations of the spectra of nanosized powders (sample nos. 1–4). Within this simple model, no considerable difference between electron paramagnetic resonance spectra of sample no. 1 (in the absence of hydrothermal treatment, Fig. 4), no. 2, and no. 3 was detected, where the half-widths Δ_1 and Δ_2 are 5–10 times larger than analogous values for the single crystal. In the spectrum of sample no. 4 with the maximum τ value, additional details (Fig. 5) appear because of a some decrease in Δ_1 and Δ_2 (to 4–7 half-widths in the single crystal). Obviously, the parameters Δ_1 and Δ_2 directly depend on the nanoparticle sizes. The crystal field parameters within the point charge model are given by the sum [14]

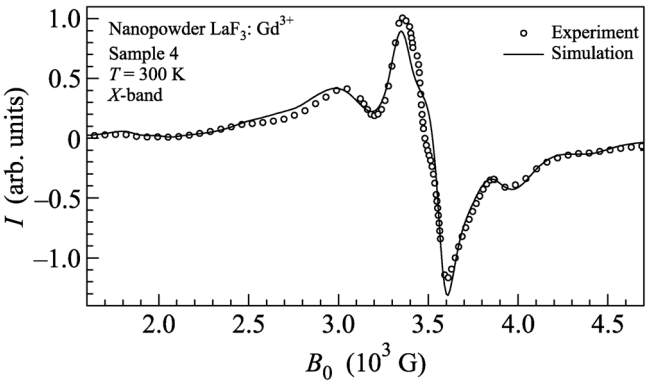

Fig. 5. Electron paramagnetic resonance spectrum of Gd^{3+} ions in the LaF_3:Gd^{3+} nanopowder (sample no. 4).

$$B_k^p = A_p^k \langle r^p \rangle K_p \gamma_p, \quad (3)$$

where $\langle r^p \rangle$ is the average value of the pth power of the radius of the electron orbit in the ground state of the Gd^{3+} ion, K_p is the reduced matrix element, and γ_p is the screening factor. The parameters A_p^k are specified by the following sum over the coordinates r_i of all ligands with charges q_i in the crystal lattice of LaF_3:

$$A_p^k = \sum_i q_i \frac{Z_p^k(r_i)}{r_i^{p+1}}, \quad (4)$$

where Z_p^k are spherical harmonics [15]. For the regular crystal, the summation over i can be expanded to the infinite crystal lattice. For the nanocrystal with the

Crystal field parameters B_p^k (in 10^{-4} cm^{-1}) and the isotropic g-factor of the effective spin Hamiltonian of the ground state of the Gd^{3+} ion in the LaF_3 crystal, and the half-width of the electron paramagnetic resonance lines Δ_i^* in different samples

Sample	B_2^0	B_2^2	B_4^0	B_4^2	B_4^4	B_4^{-2}	g	Δ_1, G	Δ_2, G
Single crystal, micropowder								21	21
Nanopowder nos. 1–3	79	9.5	0.083	–0.41	0.70	0.33	1.99	100	200
Nanopowder no. 4								80	140

* Indices 1 and 2 refer to the central line (transitions $-1/2 \leftrightarrow 1/2$) and transitions $\pm 1/2 \leftrightarrow \pm 3/2$, respectively.

cross section R, this summation is limited by a certain value r_i. For this Gd^{3+} ion located in a certain position in the nanocrystal,

$$A_p^{k(\text{nano})} = A_p^{k(\text{mono})} - \delta A_p^k. \quad (5)$$

The shift δA_p^k from the value for the single crystal is due to the contributions from the ligands located at the distances on the order of R and larger. Above, we used the point charge model, which describes adequately the contribution to the crystal field energy from the ligands at a distance exceeding the size of several unit cells. Below, we will limit ourselves to qualitative considerations [16]. Averaging over different positions of the impurity center in the nanoparticle gives $\langle \delta A_p^k \rangle = 0$. Consequently, the electron paramagnetic resonance spectra of nanopowders can be described by the same set of parameters B_p^k as the single-crystal spectra. We ignore the deformation of the nanocrystal structure and the corresponding change in the crystal field parameters as a higher order effect for particle sizes $R \geq 20$ nm. The spectral line broadening is associated with the presence of the spread of the δA_p^k parameter. The largest contribution to the crystal field comes from the parameter B_2^0 (see table). The half-width owing to the spread of B_2^0 is inversely proportional to R [16]. The ratio of the nanoparticle sizes in sample nos. 1 and 4 is estimated in terms of the half-widths Δ_1 and Δ_2 (after subtraction of their single-crystal values) as $R_1/R_4 = 1.3–1.5$. This ratio is very close to the corresponding value in the isostructural PrF_3 crystal obtained using electron microscopy [6] (39 nm/27 nm = 1.44).

Our study demonstrates reliably that the method of hydrothermal treatment can be used successfully for the preparation of nanocrystal powders with the particle size varied in a narrow range. The sizes and regularity of the structure of such particles can be determined both directly (using electron microscopy methods) and indirectly (using the estimates of the crystal field parameters and their spread). Good agreement between the calculations and measured electron paramagnetic resonance spectra of Gd^{3+} ions in LaF_3:Gd^{3+} indicate the possibility of using the LaF_3:Gd^{3+} nanopowder as a contrast agent in magnetic resonance tomography.

We are grateful to V.A. Atsarkin for the discussion of results and valuable comments. E.I.B. acknowledges the support of the Dynasty Foundation. This work was partly supported by the Russian Foundation for Basic Research (project no. 12-02-00372-a).

REFERENCES

1. J. Bridot, A. Faure, S. Laurent, C. Riviere, C. Billotey, M. Janier, V. Josserand, J. Coll, L. Elst, R. Muller, S. Roux, P. Perriat, and O. Tillement, J. Am. Chem. Soc. **129**, 5076 (2007).
2. J. S. Ananta, B. Godin, R. Sethiet, L. Moriggi, X. Liu, R. Serda, R. Krishnamurthy, R. Muthupillai, R. Bolskar, L. Helm, M. Ferrari, L. Wilson, and P. Decuzzi, Nature Nanotechnol. **5**, 815 (2010).
3. G. Liang, J. Ronald, Y. Chen, P. Pandit, M. Ma, B. Rutt, and J. Rao, Angew. Chem. Int. Ed. **50**, 6283 (2011).
4. C. Bouzigues, T. Gacoin, and A. Alexandrou, ACS Nano **5**, 8488 (2011).
5. L. Ma, W. Chen, Y. Zheng, J. Zhao, and Z. Xu, Mater. Lett. **61**, 2765 (2007).
6. E. M. Alakshin, B. M. Gabidullin, A. T. Gubaidullin, A. V. Klochkov, S. L. Korableva, M. A. Neklyudova, A. M. Sabitova, and M. S. Tagirov, arXiv:1104.0208 (2011).
7. E. M. Alakshin, R. R. Gazizulin, A. V. Egorov, A. V. Klochkov, S. L. Korableva, V. V. Kuzmin, A. S. Nizamutdinov, M. S. Tagirov, K. Kono, A. Nakao, and A. T. Gubaidullin, J. Low Temp. Phys. **162**, 645 (2011).
8. E. M. Alakshin, D. S. Blokhin, A. M. Sabitova, A. V. Klochkov, V. V. Klochkov, K. Kono, S. L. Korableva, and M. S. Tagirov, JETP Lett. **96**, 181 (2012).
9. E. M. Alakshin, R. R. Gazizulin, A. V. Klochkov, S. L. Korableva, V. V. Kuzmin, A. M. Sabitova, T. R. Safin, K. R. Safiullin, and M. S. Tagirov, JETP Lett. **97**, 579 (2013).
10. K. W. H. Stevens, Proc. Phys. Soc. A **65**, 209 (1952).
11. V. K. Sharma, J. Chem. Phys. **54**, 496 (1971).
12. D. A. Jones, J. M. Baker, and D. F. D. Pope, Proc. Phys. Soc. **74**, 249 (1959).
13. S. K. Misra, P. Mikolajczak, and S. Korczak, J. Chem. Phys. **74**, 922 (1981).
14. N. R. Lewis and S. K. Misra, Phys. Rev. B **27**, 3425 (1983).
15. N. R. Lewis and S. K. Misra, Phys. Rev. B **25**, 5421 (1982).
16. E. I. Baibekov, to be published.

Translated by L. Mosina